





Cite this: *Phys. Chem. Chem. Phys.*,  
2017, **19**, 24735

# Giant lattice expansion by quantum stress and universal atomic forces in semiconductors under instant ultrafast laser excitation†

Nian-Ke Chen,<sup>a</sup> Dong Han,<sup>b</sup> Xian-Bin Li,<sup>c</sup> \*<sup>a</sup> Feng Liu,<sup>c</sup> Junhyeok Bang,<sup>d</sup>  
Xue-Peng Wang,<sup>a</sup> Qi-Dai Chen,<sup>a</sup> Hai-Yu Wang,<sup>a</sup> Shengbai Zhang\*<sup>e</sup> and  
Hong-Bo Sun \*<sup>a</sup>

Femtosecond lasers (fs) can cause a disparity between electronic and lattice temperatures in the very short period after irradiation. In this relatively cool lattice regime, the material properties can differ drastically from those under thermal equilibrium. In particular, first-principles calculations reveal two general mechanical effects on semiconductors. Firstly, the excitation can induce a negative pressure on the lattice, causing a >10% expansion, even for superhard diamond. Secondly, it induces inhomogeneous local forces on the atoms, for both perfect and distorted lattices. In the case of phase-change-memory for Ge<sub>2</sub>Sb<sub>2</sub>Te<sub>5</sub> and GeTe alloys, such random forces cause a simultaneous phase transition from crystalline to amorphous, which enables faster data writing. These excitation effects are further supported by the time-dependent density functional theory. This work could be an important step in advancing fs laser techniques for the atomic-level control of structures, rather than relying on traditional melting or ablation approaches which often apply to much larger and non-atomic scales.

Received 10th May 2017,  
Accepted 14th August 2017

DOI: 10.1039/c7cp03103c

rs.li/pccp

## 1 Introduction

Femtosecond (fs) lasers have played a critical role in materials processing at the micro–nano-scale.<sup>1–5</sup> Fascinating two-dimensional (2D) and three-dimensional (3D) functional devices for applications in microelectronics, micro-optics, micromechanics, and micro-fluidics have been produced by incorporating fs laser processing.<sup>6–9</sup> Deep insight into the dynamics of material excitation at the fs time scale is critical for high precision control of structural geometry and chemical composition variations. The generally accepted picture of fs laser–matter interaction is the two-temperature model (TTM),<sup>10–12</sup> which divides the excitation into two stages. First, the laser energy is coupled to electrons within a very short period of time, *i.e.*, of the order of a sub-picosecond, to create electron/hole plasmas with the

lattice remaining undisturbed and cool. These excited carriers then relax during the second stage through electron–electron scattering and electron–phonon coupling, and give their energies to the lattice resulting in melting,<sup>13</sup> ablation,<sup>14</sup> or a thermal explosion.<sup>15</sup> The changes of the material properties in this model occur during the second stage. Some recent observations, however, reveal that the crystalline Ge<sub>10</sub>Sb<sub>2</sub>Te<sub>13</sub> phase can be changed to a stable amorphous state within 500 fs under exposure to a fs laser pulse.<sup>16</sup> This means that the materials can be manipulated and processed when their lattices are still cool, and it shows the prospect of creating a new phase which is otherwise difficult to obtain. Despite this fact, a quantitative understanding of the lattice behavior in the first stage is relatively limited, with a few exceptions.<sup>17–19</sup>

In this study, we found through first-principles calculations that the lattice variation is not negligible, starting from the very beginning of the fs excitation. Due to the electrons pumped from the valence band to the conductive band, the bare lattice suffers from quantum electronic stress, which is manifested as a negative pressure. Unlike the negative pressure obtained by thermal expansion, the electronic pressure causes a lattice expansion of up to 10% even at 0 K. This is quite unusual for diamond, not only because its thermal expansion is negligible but also due to the fact that obtaining a significant lattice expansion usually requires the use of a harder material, which does not naturally exist. In addition, the dynamic atomic forces due to excitation are a general phenomenon, which often drive

<sup>a</sup> State Key Laboratory on Integrated Optoelectronics, College of Electronic Science and Engineering, Jilin University, Changchun 130012, China.

E-mail: lixianbin@jlu.edu.cn, hbsun@jlu.edu.cn

<sup>b</sup> State Key Laboratory of Luminescence and Applications, Changchun Institute of Optics, Fine Mechanics and Physics, Chinese Academy of Sciences, Changchun 130033, China

<sup>c</sup> Department of Materials Science and Engineering, University of Utah, Salt Lake City, Utah 84112, USA

<sup>d</sup> Spin Engineering Physics Team, Korea Basic Science Institute (KBSI), Daejeon 305-806, South Korea

<sup>e</sup> Department of Physics, Applied Physics, & Astronomy, Rensselaer Polytechnic Institute, Troy, New York 12180, USA. E-mail: zhangs9@rpi.edu

† Electronic supplementary information (ESI) available. See DOI: 10.1039/c7cp03103c

the system into amorphization. Considering the phase change memory materials, Ge<sub>2</sub>Sb<sub>2</sub>Te<sub>5</sub> (GST) and cubic GeTe, in which the first has no lattice symmetry and the latter has a perfect centrosymmetry, the atomic forces directly trigger amorphization in both for temperatures as low as 100 K. These new findings show that the lattice response to fs excitation in the first stage may play a critical role in materials processing, which will directly benefit the quality of laser micromanufacturing.

## 2 Methods

Our calculations are based on density functional theory (DFT) within the generalized gradient approximation and the pseudopotential approximation,<sup>20,21</sup> as implemented in the VASP code.<sup>22</sup> All the studies of zinc blende semiconductors employ a 216-atom supercell. The cutoff energies are 200 eV for GaSb, 200 eV for GaAs, 240 eV for GaP, 260 eV for MgS, 200 eV for MgSe, 280 eV for ZnS, 400 eV for diamond, and 450 eV for cubic BN. For the phase change memory materials, we use a cubic rock-salt cell (including 42 Ge atoms, 44 Sb atoms, 108 Te atoms, and 22 vacancies<sup>23</sup>) for GST and a cubic rock-salt cell (including 108 Ge atoms and 108 Te atoms) for GeTe. The cutoff energies are 240 eV for static calculations and 180 eV for *ab initio* molecular dynamics (MD). A single  $\Gamma$  point is used for Brillouin zone integration. To mimic the effects of optical excitation, a fraction of the electrons are taken away from the valence band (VB) edge and replaced in the conduction band (CB) edge with fixed electron and hole occupancies (analogous to ref. 24); see the inset of Fig. 1a. This corresponds to the time domain of interest, namely, after the fs laser excitation between the band edge states but before the recombination of the electron/hole plasma. Moreover, the new distribution of the electron density after excitation is determined by DFT self-consistent calculations. During the MD simulation, the energy band changes with the evolution of the structure. The electron density then redistributes with the change of energy band, guaranteeing that the excited electrons/holes relocate to the CB/VB edges. To test the feasibility of using the fixed occupation method to evaluate

the initial mechanics by laser excitation, we also performed a calculation for two examples to determine the initial stress and force by using the time-dependent density functional theory (TDDFT),<sup>25</sup> as implemented in the code based on the SIESTA program.<sup>26–28</sup> We used norm-conserving Troullier–Martins pseudopotentials,<sup>29</sup> the Perdew–Burke–Ernzerhof (PBE) exchange–correlation function,<sup>30</sup> and a local basis set with double- $\zeta$  polarized orbitals. A real-space grid equivalent to a plane-wave cutoff of 100 Ry was adopted. A single  $\Gamma$  point was used to sample the Brillouin zone. To obtain the information of the initial excitation, we extracted the results of stress and force after a short duration of 0.24 fs in TDDFT-MD.

## 3 Results and discussion

### 3.1 Physical origin of the excitation induced quantum stress and atomic force

To understand the dynamic response, we note that the equilibrium position of the system is a strong function of excitation. The excitation breaks the ground-state balance between atoms and electrons, and thus produces mechanical stresses and forces in the materials, which dominate the structural evolution. To better understand the physical origin of the excitation induced stress and force, we briefly review the formulation below.

By definition, the stress tensor is expressed as the derivative of the total energy  $E_{\text{tot}}$  with respect to the strain  $\varepsilon_{ij}$ :

$$\sigma_{ij} = (1/V) \cdot (dE_{\text{tot}}/d\varepsilon_{ij}). \quad (1)$$

By definition, the Hellmann–Feynman force on an atom is the derivative of the total energy with respect to the atomic coordinate  $R$ :

$$F = -dE_{\text{tot}}/dR. \quad (2)$$

Based on the work by Hu *et al.*,<sup>31</sup> we assume that the variation of the electron density from  $n^0(\vec{r})$  (the ground-state density) is  $n^*(\vec{r}) = n^0(\vec{r}) + \delta n(\vec{r})$ . Then the total energy can be written as:

$$E[n^*(\vec{r})] = E[n^0(\vec{r})] + \int_V \left( \frac{\delta E[n(\vec{r})]}{\delta n(\vec{r})} \right)_{n^0} \delta n(\vec{r}) d\vec{r}, \quad (3)$$

where the first term is the ground-state energy and the second term is the energy variation due to the change in electron density. The original ground-state solid is stress free, so  $dE[n^0(\vec{r})]/d\varepsilon_{ij} = 0$ . Hu *et al.*<sup>31</sup> have derived the stress induced by electronic excitation and perturbation without applying lattice strain:

$$\begin{aligned} \sigma_{ij} &= \frac{1}{V} \frac{dE[n^*(\vec{r})]}{d\varepsilon_{ij}} \Big|_{n^0, \varepsilon_{ij}=0} \\ &= \frac{1}{V} \left\{ \int_V \left[ \frac{\partial \mu}{\partial \varepsilon_{ij}} \delta n(\vec{r}) + \mu \frac{\partial [\delta n(\vec{r})]}{\partial \varepsilon_{ij}} \right] d\vec{r} \right\}_{n^0, \varepsilon_{ij}=0} \end{aligned} \quad (4)$$

where  $\mu = \partial E[n(\vec{r})]/\partial n(\vec{r})$  is the electron chemical potential. The second term vanishes because the number of electrons is independent of strain. The stress induced by adding either electrons or holes in a semiconductor<sup>31</sup> can be written as:

$$\sigma^{e, \text{ or } h} = \Xi^{e, \text{ or } h} \times \Delta n_{e, \text{ or } h} \quad (5)$$

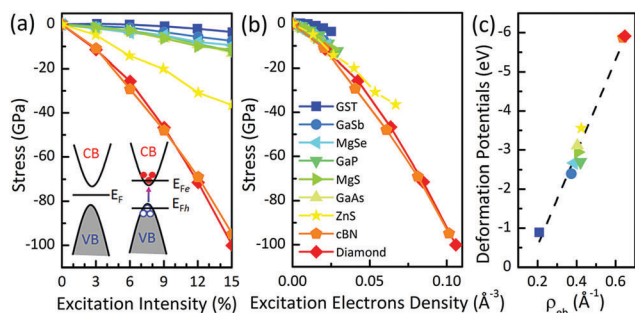


Fig. 1 (a) The stress vs. the excitation intensity in a series of semiconductors. The inset shows the band schematic in an optical excitation. (b) The stress vs. the corresponding excitation electron density. (c) The slope using a fit in (b) (i.e., the deformation potential) is proportional to the bonding strength.

(Here, a bonding electronic density  $\rho_{\text{eb}} = \frac{N_{\text{eb}}}{\text{CN} \cdot \text{BL}}$  is defined, see more details in the ESI†).

where  $\Xi^e = d\mu^e/d\varepsilon = dE_{\text{CBM}}/d\varepsilon$ , and  $\Xi^h = d\mu^h/d\varepsilon = dE_{\text{VBM}}/d\varepsilon$  are the deformation potential of the conduction band minimum (CBM) and the valence band maximum (VBM), respectively,  $\varepsilon$  is the lattice strain, and  $\Delta n_{e,\text{or }h}$  is the change in the electron (or hole) density. Here, we considered the case of true optical excitation where the same number of electrons in the CB and holes in the VB are produced at the same time during excitation. Under the adiabatic approximation of fixed energy levels, the total stress induced by both electrons and holes becomes

$$\sigma = (\Xi^e - \Xi^h) \times \Delta n = \Xi^{E_g} \times \Delta n. \quad (6)$$

In deriving eqn (6), we use the condition  $\Delta n_e = -\Delta n_h = \Delta n$ , and  $E_g = E_{\text{CBM}} - E_{\text{VBM}}$  is the intrinsic band gap of the semiconductor. In the case of strong excitation, such as by a fs laser pulse, we can further include the shift in the conduction and valence band edges associated with excitation and define the effective band gap  $E_g' = E_g + \delta_{\text{CBM}} + \delta_{\text{VBM}}$ , with

$$\sigma = \Xi^{E_g'} \times \Delta n. \quad (7)$$

Here,  $\Xi^{E_g'}$  is the effective deformation potential induced by the fs excitation (see more discussions in the ESI†) while  $\Delta n$  is the carrier density ( $\Delta N/V$ ). In other words, the stress is proportional to the excitation density. As early as 1961, Figielski observed that the stress in Ge had a linear dependence on the excitation intensity ( $\Delta N/N_{\text{tot}}$ ) in the low range ( $\ll 1\%$ ).<sup>32</sup> For a high excitation,  $\Xi^{E_g'}$  is not constant due to the variable effective band gap. However, in the current study, we will concentrate on showing that the stress is a strong function of the excitation carriers according to eqn (7).

The electronic excitation induced force on an atom  $i$  is also a function of the variation of electron density:

$$F = \left\{ - \int_V \left[ \frac{\partial \mu}{\partial R_i} \delta n(\vec{r}) + \mu \frac{\partial [\delta n(\vec{r})]}{\partial R_i} \right] d\vec{r} \right\}_{n^0, R_i=0}. \quad (8)$$

In general, the electronic excitation induced stress and force originate from the redistribution of the electron density in the solid. It should be noted that eqn (7) and (8) are used to interpret the physical origin of the stress and force. In fact, the stress and force data used in this study were calculated directly from the derivative of the total energy (obtained by DFT) according to their definitions.

### 3.2 Excitation stress in semiconductors and the stress induced giant lattice expansion

By first-principles calculations, Fig. 1a summarizes the stress induced using typical fs excitations. A series of cubic semiconductors are exemplified, where the stress tensors approximately satisfy  $\sigma_{xx} = \sigma_{yy} = \sigma_{zz}$  and the off-diagonal terms satisfy  $\sigma_{ij \neq i} \approx 0$ . As the excitation intensity increases from 0% to 15%, the stress becomes more significant and is generally compressive ( $\sigma < 0$ ). The stress is replotted with the carrier density in Fig. 1b, and the slope reflects the average excitation deformation potential ( $\Xi^{E_g'}$ ). The averaged  $\Xi^{E_g'}$  is shown in Fig. 1c and is material specific and has a positively linear dependence on the bonding electronic density ( $\rho_{\text{eb}}$ ); see more details in the ESI.†

Therefore, harder or stronger materials are more readily disturbed and produce stress under fs laser excitation.

Since the magnitude of the stress can reach up to 1/10 of the bulk modulus under feasible conditions (e.g., 5–15% excitation), this alone may be enough to cause significant changes in the lattice. Two representative cases including GST and diamond carbon are tested here. GST is a flagship candidate in nonvolatile storage technologies, namely phase change memory.<sup>33,34</sup> In general, an ultrafast laser pulse can switch GST rapidly between its high reflective state (crystalline phase) and the low reflective state (amorphous phase). GST is quite soft due to its resonant bond.<sup>35</sup> In contrast, diamond carbon is well known for its superhard characteristics, and is popular as a diamond anvil cell to produce ultrahigh pressure to compress other softer materials.<sup>36</sup> Fig. 2 shows that the volumes of both systems expand significantly after their stresses are released. Here, we call it compressive stress since the system is still in the original lattice ground state. In GST, a 15% excitation can lead to a 10% volume expansion while in diamond it is more significant and an 8% excitation is enough to produce the same volume expansion. This shows the potential for negative pressure technology, in which it could be controlled quantitatively by the excitation intensity. Usually, the most effective way to expand a lattice is to increase the kinetic energy in the atoms and enhance their inharmonic vibrations during heat transfer.<sup>37</sup> However, such expansions are small, especially in a hard material. For example, according to the volumetric thermal coefficient ( $3 \times 10^{-6} \text{ K}^{-1}$ ),<sup>38</sup> even up to the melting point ( $\sim 4000 \text{ K}$ ),<sup>39</sup> the volume of diamond increases only by  $\sim 1\%$ , which is one order smaller than that proposal here using fs laser excitation. In fact, such an unusual expansion in the lattice has also been observed recently in GST under fs laser exposure and the magnitude of the expansion was too large to be explained by the thermal effect alone.<sup>40</sup> The excitation induced stress may explain the observed large expansion. Therefore, the hypothesis stated here is feasible and possibly offers a new method to control materials over a large lattice.

The electronic structure under excitation is important in understanding the mechanical behavior. The spatial charge

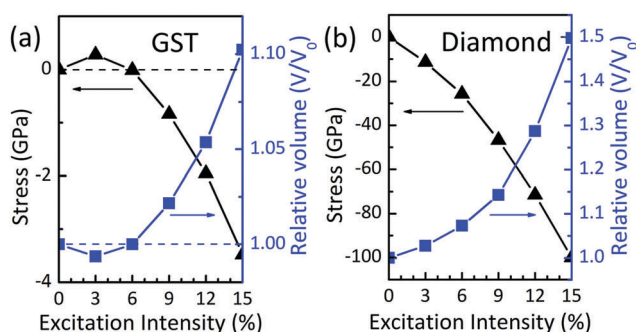


Fig. 2 The volume change is followed by a release in the excitation stress for GST (a) and diamond carbon (b). Here, a negative stress, which is equivalent to a negative pressure, leads to a lattice expansion. The volume expansions are calculated by changing the volumes to release the stresses (Fig. S1, ESI†).

density difference (S-CDD)<sup>41</sup> between the excitation state and the ground state is simulated and compared in Fig. 3. For GST, under a 3% excitation (Fig. 3a), some of the electrons around Ge were displaced (shown in blue) while Sb accepted these charges (shown in red). Specifically, for a low intensity, the cation-to-cation excitation is relatively distinct. Under a 6% excitation (Fig. 3b), Te started to donate electrons which were accepted by Sb. However, for the 9% case (Fig. 3c), Ge also started to accept the electrons from Te. Therefore, for a higher intensity (>6%) (Fig. 3c–e), the anion-to-cation excitation was dominant. However, the elemental diamond produced different results for S-CDD. As shown in Fig. 3g–k, the electrons are always removed from the bond-center site to the anti-bond site along the bond direction. A higher excitation makes this phenomenon more significant. In general, both the electrons in

the CB and holes in the VB tend to weaken the bonding and thus lead to the lattice expansion observed above. However, in the localized view, the S-CDD in the distorted GST (see the discussion in Section 3.3 about the GST lattice) was quite inhomogeneous but in diamond it was uniform. This suggests that the localized mechanics under the excitation may be different between the distorted lattice (GST) and the perfect/high-symmetry lattice (diamond).

### 3.3 Excitation force and force induced solid-to-solid amorphization in Ge<sub>2</sub>Sb<sub>2</sub>Te<sub>5</sub>

An important consideration for the local mechanics are the local forces on an atom under excitation. To quantify these, Fig. 4a shows the root mean square of the local forces in rock-salt GST and rock-salt GeTe as a function of the excitation intensity. It is well known that both the alloys are the flagship candidates in phase-change-memory technology due to their thermal transitions between the crystal and amorphous phases.<sup>33</sup> In general, rock-salt Ge<sub>2</sub>Sb<sub>2</sub>Te<sub>5</sub> has two sublattices: one is for anion Te while the other is for cation Ge, Sb, and 10% of the intrinsic vacancies. Due to their random distribution in the cation lattice, cubic GST is always locally distorted.<sup>23</sup> Conversely, rock-salt GeTe (or diamond) has a perfect lattice. It is clear that the local forces in GST increase significantly with the intensity. Fig. 4b and c shows that these local forces have random orientations and are strongly dependent on the number of neighboring vacancies. However, without any inhomogeneity in the lattice, GeTe displays no local forces at 0 K, even for an excitation intensity as high as 15%.

As a result, an instant destabilization of GST happens under optical excitation, which is demonstrated by a MD simulation. We show in Fig. 5a the evolution of the pair correlation functions. The driving force for the transition was also demonstrated by the local-force evolution in Fig. 5b. However, unexpectedly in the same 100 K MD in GeTe with 15% excitation, the zero local force in the initial state increased to the same level as GST within 300 fs, and then was constant during the whole excitation. As such, GeTe is also rapidly amorphized after 3 ps; see Fig. 5c. A negligible local force in the perfect lattice does not imply absolute stability under excitation, but indicates a local minimum (or local maximum, or saddle point) of the potential energy surface.

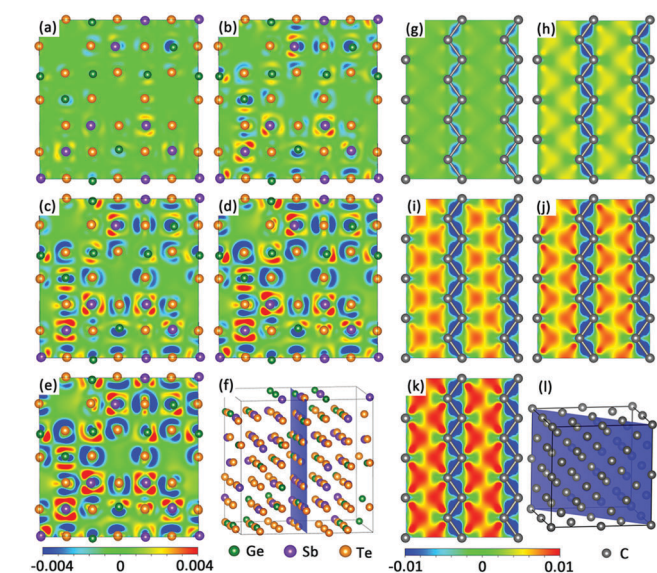


Fig. 3 The spatial charge density difference (S-CDD) between the excitation state and the ground state. A positive or negative value implies an increase in density or a decrease in density under an optical excitation, respectively. Panels (a)–(e) and (g)–(k) are the S-CDDs with 3%, 6%, 9%, 12%, and 15% excitation intensity, respectively for GST and diamond carbon. Panels (f) and (l) highlight the cutting planes for the S-CDD analysis. The units in the color scale bar is e Bohr<sup>-3</sup>.

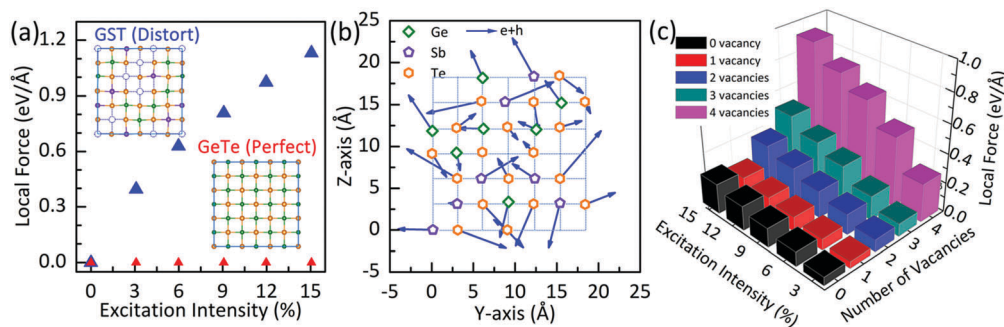


Fig. 4 (a) Atomic local forces in the distorted rock-salt GST and the perfect rock-salt GeTe under optical excitation. (b) Inhomogeneous local forces under optical excitation (15%) in GST: the projected forces on a (100) plane. (c) Magnitude of the local force on Te in GST vs. either the excitation intensity or the number of nearest cation vacancies.

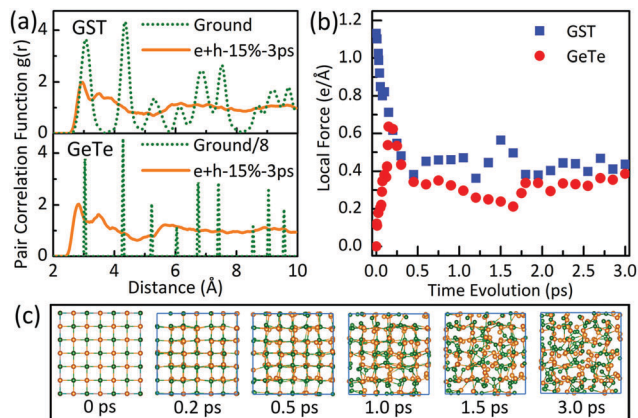


Fig. 5 (a) Pair correlation function (PCF) before and after a 3 ps MD with a 15% optical excitation at 100 K for rock-salt GST and rock-salt GeTe. (b) Evolution of the LF during the optical excitation. (c) The structural snapshots at the different stages under excitation for GeTe.

Here a tiny thermal fluctuation (in form of an atomic vibration), even at a temperature as low as 100 K, can trigger the hidden local forces for the phase change. In fact, the temperature here is far below the required melting point to realize data writing on GST or GeTe through a typical melting–quenching amorphization process.<sup>33</sup> Therefore, the local force is a universal effect under the optical excitation. There are several pump–probe experiments which have shown that GST irradiated by an ultrafast laser can transform into its amorphous state without turning into its liquid state.<sup>42–45</sup> More recently, an experiment based on time-resolved X-ray diffraction also revealed a decrease in the peak intensity before the shift of peak position which indicates<sup>46</sup> a phase transition before the thermal expansion. This solid-to-solid amorphization of GST can be explained by the randomly distributed excitation forces.

### 3.4 Discussion and outlook

The TTM assumes that the response time of the electrons to the excitation is much faster than the response time of the atoms. In the first stage of the TTM, the lattice remains cold while the temperature of the electrons increases rapidly. In the second stage, the temperature of the lattice gradually increases *via* electron–phonon coupling and finally leads to phase transitions. In the TTM, thermal effects are significant. However, our results indicate that substantial stresses and forces can be produced instantly by excitation, and that a phase transition can take place when the lattice is still cold. In our results, the mechanical effects (stress and force) are the leading contributors. It should be noted that our results are not completely unfavorable to the TTM. Actually, the work reported here is based on the two-temperature assumption since the results exhibited the behavior of the lattice in the first stage of the TTM. However, the time-scales of the second stage are out of the scope of the work presented here.

Both the expansion and amorphization induced by excitation are different from those induced by thermal effects. The electronic excitation weakens the bonds and results in a new equilibrium

position for the lattice. The expansion comes from the change in the potential energy surfaces which is different from the inharmonic effect induced by thermal expansion. Also, the excitation induced expansion can be much larger than the normal thermal expansion, especially in super-hard materials, such as diamond. Similar to the stress, the force also comes from the change in the potential energy surfaces. Due to the low symmetry of the distorted GST lattice, the directions of the forces are randomly distributed under excitation. They naturally lead to the amorphization without melting. Compared to thermal melting, this solid-to-solid amorphization is completed with less atomic diffusion, which can suppress the phase separation of multi-component alloys.

Although recent reports claimed that electron–phonon scattering occurs on a 10–100 fs timescale,<sup>47,48</sup> the materials still need several picoseconds before the carriers and the lattice reach thermal equilibrium.<sup>49</sup> The electronic excitation induced stress and forces must have significant roles in the phase change. If the lattice temperature can be managed, *e.g.*, by extracting the heat generated during the relaxation of the excited carriers or even precooling the lattice before excitation, not only more athermal properties may be retained upon cooling of the excited carriers, but there could also be other potential benefits such as the suppression of the various effects due to entropy.

### 3.5 Effectiveness of the method used in this study

Finally, we discuss the method and its effectiveness in evaluating the initial force. Although our method is not ideal for the calculation of excited states, it can offer feasible conclusions. For example, Giret *et al.* have discussed the non-thermal phase transition in tungsten by phonon spectra in excited states using fixed occupation.<sup>50</sup> Recently, J Bang *et al.* have presented a new non-radiative recombination mechanism by calculating the electronic energy level evolutions and energy barriers for the Frenkel pair defect formation in excited states in a similar way.<sup>51</sup> Undoubtedly, there are some more effective methods to examine excitation, such as methods based on the frame of GW-BSE<sup>52</sup> and TDDFT.<sup>25</sup> In order to test the effectiveness of the

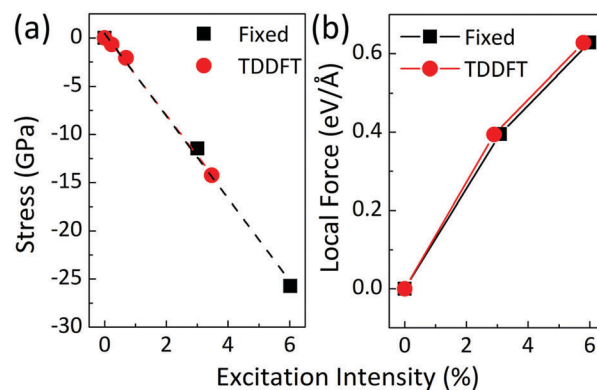


Fig. 6 Comparison of the results between fixed occupation and TDDFT. (a) Stress in diamond and (b) atom force in GST under excitation. The black solid squares are the results of the fixed occupation method. The red solid circles are results of the TDDFT method. The dashed lines in (a) are the results of linear fitting.

results using fixed occupation to mimic excitation, we carried out TDDFT-MD for the two examples: diamond and GST. To obtain the information of the instant mechanics under excitation, we extracted the results of the stress and forces after a short duration of 0.2419 fs in TDDFT MD. Fig. 6 shows the consistent results between those from fixed occupation and from TDDFT. Therefore, the initial stress and force under excitation in the present study are valid and plausible.

## 4 Conclusions

In summary, first-principles calculations reveal the significance of dynamic effects in the non-thermal time domain which can be fundamentally different from those in the thermal time domain. The most predominant effects are the ultrahigh negative pressures of the order of  $-100$  GPa on the cold lattice, which are not achieved by other means, and the existence of local atom forces which are insensitive to crystal symmetry due to the presence of lattice imperfections, such as defects or lattice vibrations which lead to possible ultrafast lattice amorphization. A negative high-pressure may lead to low-coordination phases of the exotic physical properties such as the recently proposed pure-carbon Weyl semimetal with an average coordination number of less than four,<sup>53</sup> opposite to that of positive high-pressure physics. Conversely, ultrafast amorphization induced by the excitation forces<sup>54</sup> can be a benefit to related fields, such as phase-change memory,<sup>55,56</sup> due to the ability of rapid data writing. The present study is an important step in advancing fs laser techniques towards the atomic-level control of material structures, rather than relying on the traditional melting, ablation, and/or drilling approaches, which apply to much larger and non-atomic scales.

## Conflicts of interest

There are no conflicts to declare.

## Acknowledgements

Work at JLU, China, was supported by the National Natural Science Foundation of China (NSFC) and National key research and development program under Grant #91423102, #11374119, #61590930, #2017YFB1104300, #2017YFB1104601, and 973 Program (No. 2014CB921303). Work at RPI was supported by the US Department of Energy under Grant No. DE-SC0002623. JB was supported by KBSI grant D37614. The supercomputer time was provided by HPCC at JLU. N.-K. Chen and D. Han contributed equally to this work.

## References

- M. Haque, K. K. Lee, S. Ho, L. A. Fernandes and P. R. Herman, *Lab Chip*, 2014, **14**, 3817–3829.
- K.-S. Lee, R. H. Kim, D.-Y. Yang and S. H. Park, *Prog. Polym. Sci.*, 2008, **33**, 631–681.
- K. K. Seet, V. Mizeikis, S. Matsuo, S. Juodkazis and H. Misawa, *Adv. Mater.*, 2005, **17**, 541–545.
- M. Malinauskas, A. Žukauskas, S. Hasegawa, Y. Hayasaki, V. Mizeikis, R. Buividas and S. Juodkazis, *Light: Sci. Appl.*, 2016, **5**, e16133.
- L. Wang, Q. Li, H.-Y. Wang, J. C. Huang, R. Zhang, Q.-D. Chen, H.-L. Xu, W. Han, Z. Z. Shao and H.-B. Sun, *Light: Sci. Appl.*, 2015, **4**, e245.
- H.-B. Jiang, Y.-L. Zhang, D.-D. Han, H. Xia, J. Feng, Q.-D. Chen, Z.-R. Hong and H.-B. Sun, *Adv. Funct. Mater.*, 2014, **24**, 4595–4602.
- Y. L. Sun, Q. Li, S. M. Sun, J. C. Huang, B. Y. Zheng, Q. D. Chen, Z. Z. Shao and H. B. Sun, *Nat. Commun.*, 2015, **6**, 8612.
- L. Wang, H. Y. Wang, Y. Wang, S. J. Zhu, Y. L. Zhang, J. H. Zhang, Q. D. Chen, W. Han, H. L. Xu, B. Yang and H. B. Sun, *Adv. Mater.*, 2013, **25**, 6539–6545.
- D. Yin, J. Feng, R. Ma, Y. F. Liu, Y. L. Zhang, X. L. Zhang, Y. G. Bi, Q. D. Chen and H. B. Sun, *Nat. Commun.*, 2016, **7**, 11573.
- P. B. Allen, *Phys. Rev. Lett.*, 1987, **59**, 1460–1463.
- S. I. Anisimov, B. L. Kapeliovich and T. L. Perel'man, *Sov. Phys. JETP*, 1974, **39**, 375–377.
- M. I. Kaganov, I. M. Lifshitz and L. V. Tanatarov, *Sov. Phys. JETP*, 1957, **4**, 173.
- S. S. Wellershoff, J. Hohlfeld, J. Güdde and E. Matthias, *Appl. Phys. A: Mater. Sci. Process.*, 1999, **69**, S99–S107.
- V. Schmidt, W. Husinsky and G. Betz, *Appl. Surf. Sci.*, 2002, **197–198**, 145–155.
- A. Vailionis, E. G. Gamaly, V. Mizeikis, W. Yang, A. V. Rode and S. Juodkazis, *Nat. Commun.*, 2011, **2**, 445.
- M. Konishi, H. Santo, Y. Hongo, K. Tajima, M. Hosoi and T. Saiki, *Appl. Opt.*, 2010, **49**, 3470–3473.
- E. N. Glezer, Y. Siegal, L. Huang and E. Mazur, *Phys. Rev. B: Condens. Matter Mater. Phys.*, 1995, **51**, 9589–9596.
- K. Sokolowski-Tinten, J. Bialkowski and D. von der Linde, *Phys. Rev. B: Condens. Matter Mater. Phys.*, 1995, **51**, 14186–14198.
- P. Stampfli and K. H. Bennemann, *Phys. Rev. B: Condens. Matter Mater. Phys.*, 1990, **42**, 7163–7173.
- J. P. Perdew and Y. Wang, *Phys. Rev. B: Condens. Matter Mater. Phys.*, 1992, **45**, 13244–13249.
- D. Vanderbilt, *Phys. Rev. B: Condens. Matter Mater. Phys.*, 1990, **41**, 7892–7895.
- G. Kresse and J. Furthmüller, *Phys. Rev. B: Condens. Matter Mater. Phys.*, 1996, **54**, 11169.
- T. Matsunaga, N. Yamada and Y. Kubota, *Acta Crystallogr., Sect. B: Struct. Sci.*, 2004, **60**, 685–691.
- P. Tangney and S. Fahy, *Phys. Rev. B: Condens. Matter Mater. Phys.*, 2002, **65**, 054302.
- E. Runge and E. K. U. Gross, *Phys. Rev. Lett.*, 1984, **52**, 997–1000.
- S. Meng and E. Kaxiras, *J. Chem. Phys.*, 2008, **129**, 054110.
- J. M. Soler, E. Artacho, J. D. Gale, A. García, J. Junquera, P. Ordejón and D. Sánchez-Portal, *J. Phys.: Condens. Matter*, 2002, **14**, 2745.
- O. Sugino and Y. Miyamoto, *Phys. Rev. B: Condens. Matter Mater. Phys.*, 1999, **59**, 2579.

- 29 N. Troullier and J. L. Martins, *Phys. Rev. B: Condens. Matter Mater. Phys.*, 1991, **43**, 1993–2006.
- 30 J. P. Perdew, K. Burke and M. Ernzerhof, *Phys. Rev. Lett.*, 1996, **77**, 3865–3868.
- 31 H. Hu, M. Liu, Z. F. Wang, J. Zhu, D. Wu, H. Ding, Z. Liu and F. Liu, *Phys. Rev. Lett.*, 2012, **109**, 055501.
- 32 T. Figielski, *Phys. Status Solidi*, 1961, **1**, 306–316.
- 33 M. Wuttig and N. Yamada, *Nat. Mater.*, 2007, **6**, 824–832.
- 34 N. Yamada, E. Ohno, K. Nishiuchi, N. Akahira and M. Takao, *J. Appl. Phys.*, 1991, **69**, 2849–2856.
- 35 K. Shportko, S. Kremers, M. Woda, D. Lencer, J. Robertson and M. Wuttig, *Nat. Mater.*, 2008, **7**, 653–658.
- 36 H. Liu, L. Wang, X. Xiao, F. De Carlo, J. Feng, H. K. Mao and R. J. Hemley, *Proc. Natl. Acad. Sci. U. S. A.*, 2008, **105**, 13229–13234.
- 37 T. H. K. Barron, J. G. Collins and G. K. White, *Adv. Phys.*, 1980, **29**, 609–730.
- 38 T. Sato, K. Ohashi, T. Sudoh, K. Haruna and H. Maeta, *Phys. Rev. B: Condens. Matter Mater. Phys.*, 2002, **65**, 092102.
- 39 A. A. Correa, S. A. Bonev and G. Galli, *Proc. Natl. Acad. Sci. U. S. A.*, 2006, **103**, 1204–1208.
- 40 P. Fons, P. Rodenbach, K. V. Mitrofanov, A. V. Kolobov, J. Tominaga, R. Shayduk, A. Giussani, R. Calarco, M. Hanke, H. Riechert, R. E. Simpson and M. Hase, *Phys. Rev. B: Condens. Matter Mater. Phys.*, 2014, **90**, 094305.
- 41 A. V. Kolobov, P. Fons, J. Tominaga and S. R. Ovshinsky, *Phys. Rev. B: Condens. Matter Mater. Phys.*, 2013, **87**, 165206.
- 42 P. Fons, H. Osawa, A. V. Kolobov, T. Fukaya, M. Suzuki, T. Uruga, N. Kawamura, H. Tanida and J. Tominaga, *Phys. Rev. B: Condens. Matter Mater. Phys.*, 2010, **82**, 041203.
- 43 X. B. Li, X. Q. Liu, X. D. Han and S. B. Zhang, *Phys. Status Solidi B*, 2012, **249**, 1861–1866.
- 44 J. Siegel, W. Gawelda, D. Puerto, C. Dorronsoro, J. Solis, C. N. Afonso, J. C. G. de Sande, R. Bez, A. Pirovano and C. Wiemer, *J. Appl. Phys.*, 2008, **103**, 023516.
- 45 J. Siegel, A. Schropp, J. Solis, C. N. Afonso and M. Wuttig, *Appl. Phys. Lett.*, 2004, **84**, 2250–2252.
- 46 K. V. Mitrofanov, P. Fons, K. Makino, R. Terashima, T. Shimada, A. V. Kolobov, J. Tominaga, V. Bragaglia, A. Giussani, R. Calarco, H. Riechert, T. Sato, T. Katayama, K. Ogawa, T. Togashi, M. Yabashi, S. Wall, D. Brewe and M. Hase, *Sci. Rep.*, 2016, **6**, 20633.
- 47 M. Bernardi, D. Vigil-Fowler, J. Lischner, J. B. Neaton and S. G. Louie, *Phys. Rev. Lett.*, 2014, **112**, 257402.
- 48 C. A. Rozzi, S. M. Falke, N. Spallanzani, A. Rubio, E. Molinari, D. Brida, M. Maiuri, G. Cerullo, H. Schramm, J. Christoffers and C. Lienau, *Nat. Commun.*, 2013, **4**, 1602.
- 49 S. K. Sundaram and E. Mazur, *Nat. Mater.*, 2002, **1**, 217–224.
- 50 Y. Giret, S. L. Daraszewicz, D. M. Duffy, A. L. Shluger and K. Tanimura, *Phys. Rev. B: Condens. Matter Mater. Phys.*, 2014, **90**, 094103.
- 51 J. Bang, Y. Y. Sun, J. H. Song and S. B. Zhang, *Sci. Rep.*, 2016, **6**, 24404.
- 52 S. Ismail-Beigi and S. G. Louie, *Phys. Rev. Lett.*, 2003, **90**, 076401.
- 53 Y. Chen, Y. Xie, S. A. Yang, H. Pan, F. Zhang, M. L. Cohen and S. Zhang, *Nano Lett.*, 2015, **15**, 6974–6978.
- 54 X.-B. Li, X. Q. Liu, X. Liu, D. Han, Z. Zhang, X. D. Han, H.-B. Sun and S. B. Zhang, *Phys. Rev. Lett.*, 2011, **107**, 015501.
- 55 N.-K. Chen, X.-B. Li, X.-P. Wang, M.-J. Xia, S.-Y. Xie, H.-Y. Wang, Z. Song, S. B. Zhang and H.-B. Sun, *Acta Mater.*, 2015, **90**, 88–93.
- 56 X.-P. Wang, X.-B. Li, N.-K. Chen, Q.-D. Chen, X. D. Han, S. B. Zhang and H.-B. Sun, *Acta Mater.*, 2017, **136**, 242–248.